

The origin of the maximum drag reduction asymptote

George H. Choueiri, Jose M. Lopez, and Björn Hof

Institute of Science and Technology Austria, 3400 Klosterneuburg, Austria

(Dated: February 3, 2023)

The drag of turbulent flows can be drastically decreased by addition of small amounts of high molecular weight polymers. While drag reduction initially increases with polymer concentration, it eventually saturates to what is known as the maximum drag reduction (MDR) asymptote; this asymptote is generally attributed to the dynamics being reduced to a marginal yet persistent state of subdued turbulent motion. Contrary to this accepted view we will show in the following that for an appropriate choice of parameters polymers can reduce the drag beyond the suggested asymptotic limit, eliminating turbulence and giving way to laminar flow. However at higher polymer concentrations the laminar state becomes unstable, resulting in a fluctuating flow with the characteristic drag of the MDR asymptote. The asymptotic state is hence dynamically disconnected from ordinary turbulence.

In pipe and channel flows turbulence is often responsible for more than 90% of the friction losses. A very efficient and often used method to reduce this frictional drag is by addition of small amounts of long chain polymers. Since its discovery more than 60 years ago this effect has been studied extensively and various theories have been put forward to explain the mechanism of drag reduction (DR). It is commonly found that DR increases with polymer concentration but eventually saturates to the MDR asymptote [1], as shown in Fig. 1a. All studies to date suggest that regardless of polymer concentration this limit cannot be overcome [2–4]. The MDR asymptote is found to be identical for different types of polymers and polymer solvent combinations [1]. Based on these observations the general view is that polymers decrease turbulent activity (either via elastic [5] or viscous effects [6] or both) and that eventually turbulence is reduced to a marginal state which corresponds to the MDR asymptote. More explicitly it has been argued [4, 7] that turbulence is minimized to the edge between laminar and turbulent motion. It is however not clear how turbulence can persist in this limit. In purely Newtonian flow the edge is intrinsically unstable and separates initial conditions that go turbulent from those that collapse back to laminar and it has not been shown if and how this state would become stable due to the action of polymers. An alternative interpretation of the MDR state has been given more recently [8], where it has been observed that with increasing polymer concentration a different instability sets in; due to its occurrence at finite inertia and the elastic nature of the polymers it has been dubbed elasto-inertial instability. This instability has been observed independently in direct numerical simulations [9] and in laboratory experiments [8]. In the experimental study it could be shown that the elasto-inertial instability strictly arises at Reynolds numbers below those at which the MDR asymptote is assumed and that at the same time the transition to turbulence is delayed. Also Samanta et al. observed (in agreement with

earlier studies [10, 11] that for moderately high polymer concentrations disordered, chaotic motion would set in at Reynolds numbers ($Re \approx 900$) much below those at which turbulence can be observed in Newtonian fluids ($Re \approx 2000$). Based on these observations Samanta et al. proposed that on MDR the dynamics are driven by the elasto-inertial instability while Newtonian type turbulence (NTT) is eliminated before reaching MDR and they dubbed the corresponding dynamical state elasto-inertial turbulence (EIT). In the following we will demonstrate that polymers can for an appropriate choice of parameters eliminate fully turbulent motion. For increasing polymer concentration the laminar flow eventually becomes unstable again giving rise to the MDR state, which is hence disconnected from NTT. As will be shown, flows in the asymptotic drag limit at high Reynolds numbers structurally differ from NTT and at the same time closely agree with the characteristic streak patterns resulting from EIT at Reynolds numbers well below the threshold for NTT.

Experiments are carried out for pipe flow with water as the base fluid. A concentrated polymer solution was injected into the water at the pipe entrance, and the injection rate determined the polymer concentration downstream (see supplement for details). In the first set of experiments the Reynolds number was held fixed at 5200 starting from Newtonian flow where the friction factor is found to agree with the Blasius law. When the concentration, C , is increased in distinct steps from 0 parts per million (ppm), by weight, to a maximum of 60ppm the friction factor is observed to monotonically decrease and eventually settle on the maximum drag reduction asymptote (Fig. 1a – inset). Note that the addition of polymers causes a viscosity increase in the fluid which has been measured and is taken into account for the quoted Reynolds number values for all the measurements reported. While the polymer solution is shear thinning the measurements are carried out at large shear rates where the viscosity dependence is small

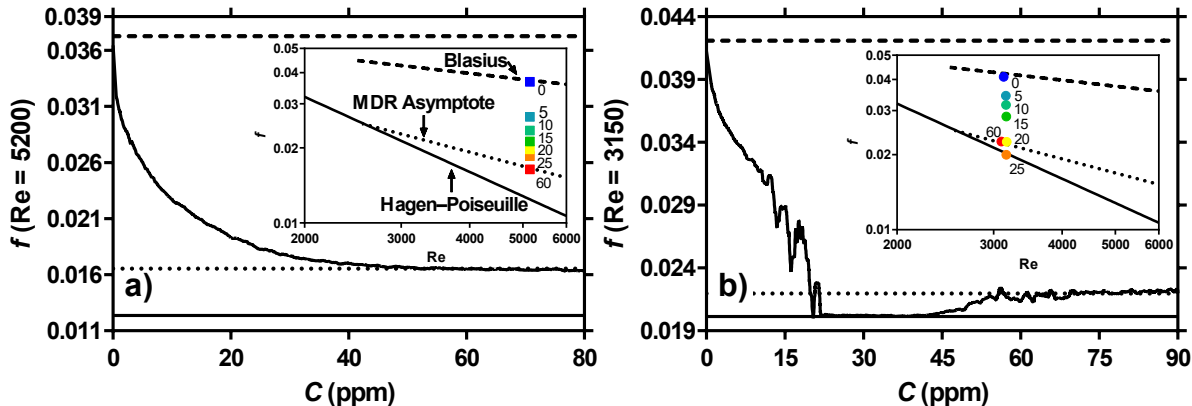


FIG. 1. The main figures show the friction factor as a function of continuously increasing polymer concentration while the insets show the friction factor at fixed concentrations as a function of Reynolds number.

[8]. When the experiment is repeated and C is increased linearly from 0 to 80ppm (over a time span of $\approx 60,000$ advective time units in a quasi-steady fashion – Fig. 1a), the continuous decrease of the friction factor and the monotonic approach towards MDR (≈ 48 ppm) are clearly seen. This observation precisely complies with the standard picture of polymer drag reduction and its asymptotic limit (see Fig. 3 in [3]). A very different scenario is observed when Re is set to 3150 (Fig. 1b – inset). Again beginning on the Blasius curve for NTT an increase in polymer concentration to 20ppm appears to reduce the friction factor to the predicted MDR value however a further increase to 25ppm pushes the friction factor below what was believed to be the limiting threshold in polymer drag reduction and recovers the laminar (Hagen-Poiseuille) value. In addition measured fluctuation levels drop to the level of instrument noise. An additional increase in polymer concentration surprisingly destabilizes the laminar flow: fluctuations increase and the friction factor increases to the “maximum” drag reduction asymptote (60ppm). While friction factors for 20 and 60ppm are almost identical and comply with the MDR value (also the time averaged velocity profiles match, not shown), structurally the flows are very different (Fig. 2b v.s. e, f). In these figures red and blue mark regions that strongly deviate from the mean streamwise speed (i.e. streaks). At 20ppm the flow is intermittent consisting of localized bursts of activity separated by much more quiescent regions. At $C > 50$ ppm however the entire flow is in a fluctuating state (Fig. 2e, f), but notably fluctuation levels are much reduced when compared to the bursts at 20ppm. This picture is confirmed when the concentration is increased continuously at a slow rate (from 0 to 90ppm over the course of $\approx 60,000$ advective time units – Fig. 1b) while Re is held fixed at $Re = 3150$. The friction factor

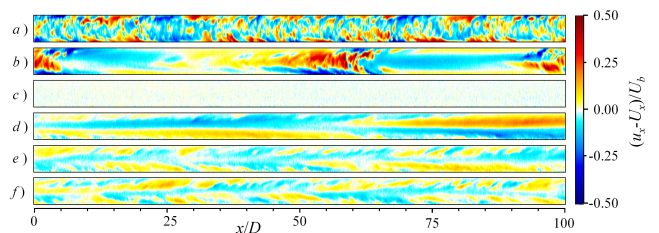


FIG. 2. Streamwise velocity deviations with respect to the mean flow profile. High speed streaks appear in red, low speed streaks in blue. The velocity field was obtained from PIV images taken in a cross-sectional plane $\sim 3D$ in length. The larger structures are then reconstructed by assuming Taylor’s frozen turbulence hypothesis; i.e. assuming that turbulence is advected downstream quickly and changes in time are slow. Images taken at different times are assembled and matched to regain the spatial structure. Measurements are carried out at $Re = 3150$ and polymer concentrations of: a) 0ppm b) 20ppm c) 30ppm d) 50ppm e) 100ppm f) 150ppm. Figure scaled to 20% in the horizontal direction. u_x is the local instantaneous streamwise velocity, U_x the average streamwise velocity and U_b the bulk velocity.

decreases gradually and close to 20ppm drops more steeply to the laminar flow value. Laminar flow persists up to about 40ppm and here the friction factor begins to increase until it settles to the MDR value for $C > 55$ ppm.

To elucidate the qualitative difference in the drag reduction scenario observed at the two different Reynolds numbers presented in Fig. 1 we carry out a detailed investigation of the Reynolds number – polymer concentration parameter space. In particular we observe that the onset of turbulence is delayed (left lower branch in Fig. 3) by the action of polymers (in agreement with [8]). While for Samanta et al. the delay only extended

to parameters where flows at most are spatio-temporally intermittent ($Re \approx 2600$) in the present case the delay extends to Reynolds numbers ($Re \approx 4000$) where in the Newtonian case turbulence is space filling ($Re \gtrsim 2800$) and assumes its characteristic friction (Blasius) scaling. When surpassing the stability boundary with increasing Re , turbulence in this regime ($C \lesssim 20\text{ppm}$) sets in in the form of localized turbulent structures (puffs) and subsequently to growing turbulent structures, commonly referred to as slugs. Like the onset of puffs the onset of slugs is equally delayed. At higher concentrations ($\gtrsim 30\text{ppm}$) a qualitatively different instability is encountered. Here fluctuations set in more uniformly in space (Fig. 2d) lacking the spatial intermittent character of the Newtonian transition scenario. This observation is in qualitative agreement with the elasto-inertial instability reported by Samanta et al. At higher concentrations this instability occurs at Re distinctly below the lowest Re where ordinary turbulence would be observed in Newtonian flow.

Starting from Newtonian turbulence for $Re \leq 4000$ (Fig. 3 – Blasius line on the left) and increasing polymer concentration, fully turbulent motion becomes unstable and returns to a regime of localized turbulent patches interspersed by more quiescent regions. Upon further increase in concentration (for $Re \lesssim 3600$) the localized turbulent structures are found to collapse and the flow completely relaminarizes. This scenario is the inverse of the familiar turbulence transition scenario in Newtonian pipe flow where turbulence first appears in the form of localized patches (first puffs then slugs) and only upon further increase in Re fully turbulent flow becomes stable [12]. In this regime the suppression of turbulence takes place before the polymer driven “elasto-inertial” instability occurs. At somewhat larger Reynolds numbers ($3600 < Re < 4500$) turbulence breaks up into localized puffs / slugs, however before complete relaminarisation is observed the instability to EIT occurs resulting in a mixed state which then eventually approaches MDR. At higher Re ($Re > 4500$) the scenario seemingly follows the traditional view of MDR where NTT is continuously suppressed by the action of polymers and the friction factor eventually settles to MDR. However what has been overlooked in previous studies is that at intermediate concentrations elasto-inertial instability sets in before MDR is reached.

The reverse transition from fully turbulent flow to localized slugs and puffs for Re ($Re < 4500$) and eventually laminar flow (for $Re < 3400$) and the fact that onset of the elasto-inertial instability is always encountered prior to the final approach to MDR raise the question if also at larger Re NTT is eventually fully suppressed as the polymer concentration is increased. In order to elucidate this question we will in the following compare the flow structure in the MDR limit for different Reynolds numbers. When comparing flow structures

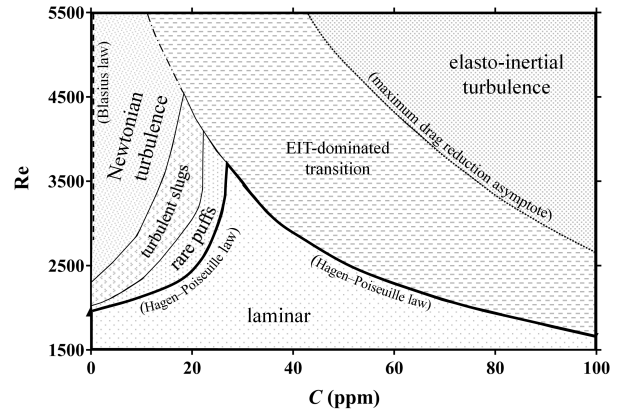


FIG. 3. State map for Reynolds number versus polymer concentrations.

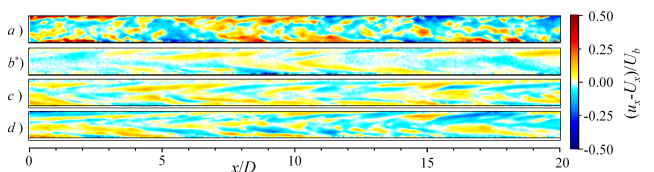


FIG. 4. Streamwise velocity deviations with respect to the mean flow profile for various Reynolds numbers and polymer concentrations. a) $Re=5200$ (0ppm) b*) $Re=1000$ (70ppm 50% glycerol) c) $Re=5200$ (125ppm) d) $Re=10000$ (68ppm).

between Newtonian (Fig. 2a) and MDR (Fig. 2f) for flow at $Re = 3150$, it is apparent that the streak pattern characteristic for NTT is virtually absent in the MDR flow. In the latter case only weak, much more elongated streaks are present that are slightly inclined with respect to the flow direction. As shown above these structures arise after NTT has been eliminated and are a consequence of the elasto-inertial instability, directly arising from laminar flow.

The MDR flow at $Re = 5200$ and 10000 at 125ppm and 68ppm respectively (Fig. 4c, d) qualitatively resembles that at $Re = 3150$ (Fig. 2e, f.) Also here the characteristic streak patterns of NTT have disappeared and only weak, inclined streaks are visible. Overall the resemblance of flow structures on MDR for the three Reynolds numbers show that MDR has characteristic features that are independent of Re . To further illustrate this point, we increased the viscosity using a 50% glycerol solution as to trigger the elasto-inertial instability at Re below that which can sustain NTT (i.e. 1000 in this case – Fig. 4b*) and we again observe low amplitude, inclined streaks similar to those on MDR at higher Re . Since the flows at $Re = 1000$ and 3150 are clearly disconnected and distinct from NTT and result solely from the elasto-inertial instability, we propose that also at $Re = 5200$ and 10000

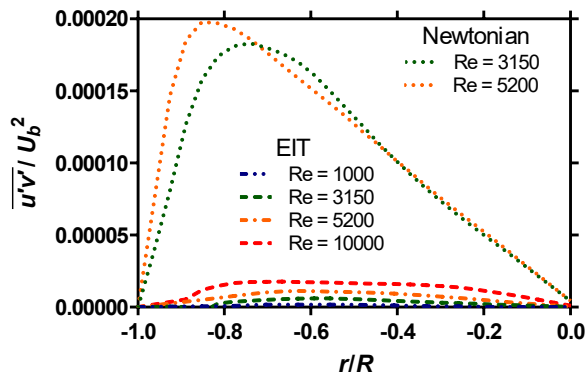


FIG. 5. Reynolds stresses for NTT and EIT normalized by the square of the bulk flow velocity.

(where MDR is approached in the usual manner) NTT is eventually suppressed and replaced by elasto-inertial turbulence only that here the eventual state is preceded by a co-existence phase rather than by relaminarisation.

While the friction factor obtained in simulations of elasto-inertial turbulence [8] matches well with the experimental measurements a direct comparison of the flow structures characterizing this flow regime is not straightforward. Simulated EIT is dominated by small scale vortical structures localized very near the wall and PIV measurements cannot resolve small spatial scales in this region. In turn due to the high computational cost of viscoelastic simulations these were performed using short axial domains which fail to capture the elongated streaks observed in the experiments. Future research should focus on confirming experimentally the existence of these vortices and clarifying their connection to the observed streaks.

Finally we computed the Reynolds stresses $\overline{u'v'}$, where u' and v' are the velocity fluctuations in the streamwise and radial direction respectively. As shown in Fig. 5 flows in the MDR (/EIT) limit have markedly lower Reynolds stresses than their Newtonian counterparts (in agreement with earlier Reynolds stress measurements at MDR [13]). We argue that the much lower Reynolds stress level distinguishes flows in the MDR limit as a separate dynamical state.

An aspect of interest for applications is that the relaminarized flow at $Re = 3150$ is not only stable to infinitesimal perturbations but also finite amplitude perturbations swiftly decay. Hence here the full drag reduction potential is achieved and remains robust to disturbances. In larger pipe diameters where shear rates are lower the elasto-inertial instability is expected to appear only at larger Re , consequently the relaminarisation interval prior to MDR may shift to larger Reynolds numbers where the drag reduction would be

considerably larger.

-
- [1] P. Virk, H. Mickley, and K. Smith, *Journal of Applied Mechanics* **37**, 488 (1970).
 - [2] K. R. Sreenivasan and C. M. White, *Journal of Fluid Mechanics* **409**, 149 (2000).
 - [3] C. M. White and M. G. Mungal, *Annu. Rev. Fluid Mech.* **40**, 235 (2008).
 - [4] L. Xi and M. D. Graham, *Physical review letters* **108**, 028301 (2012).
 - [5] M. Tabor and P. De Gennes, *EPL (Europhysics Letters)* **2**, 519 (1986).
 - [6] J. L. Lumley, *Annual Review of Fluid Mechanics* **1** (1969).
 - [7] I. Procaccia, V. S. Lvov, and R. Benzi, *Reviews of Modern Physics* **80**, 225 (2008).
 - [8] D. Samanta, Y. Dubief, M. Holzner, C. Schäfer, A. N. Morozov, C. Wagner, and B. Hof, *Proceedings of the National Academy of Sciences* **110**, 10557 (2013).
 - [9] Y. Dubief, V. E. Terrapon, and J. Soria, *Physics of Fluids* **25**, 110817 (2013).
 - [10] A. Ram and A. Tamir, *Journal of Applied Polymer Science* **8**, 2751 (1964).
 - [11] R. Little and M. Wiegard, *Journal of Applied Polymer Science* **14**, 409 (1970).
 - [12] D. Barkley, B. Song, V. Mukund, G. Lemoult, M. Avila, and B. Hof, *Nature* **526**, 550 (2015).
 - [13] M. Warholic, H. Massah, and T. Hanratty, *Experiments in fluids* **27**, 461 (1999).

SUPPLEMENTAL MATERIAL

Experiments are carried out in a $D = 10\text{mm}$ (where D is the pipe diameter) glass pipe with a total length of $646D$ using water at 296K as base for the working fluid (see Fig. 6). The main flow is fed from an elevated water reservoir of adjustable height (generally set between 2-3m above the outlet of the setup) which combined with a needle valve preceding the outlet allowed for precise flow rate control. Flow enters the pipe from an enlarged mixing chamber through a flush edge entrance and is further perturbed by a span-length 2mm pin $2.3D$ downstream from the inlet. In this configuration, Newtonian flow becomes fully turbulent for $Re > 2800$. For lower Re ($1900 < Re < 2800$) the flow is dominated by spatio-temporal intermittency, i.e. laminar and turbulent regions co-exist. Fully turbulence here specifies that prior to the first pressure tap ($484D$ from the inlet) the entire flow is in disordered motion and that the friction factor follows the Blasius friction scaling for Newtonian turbulence. The mixing chamber, which is a short $2D$ wide section of pipe, contains a resistance temperature detector (RTD) element and a polymer-injection port which connects to a pair of

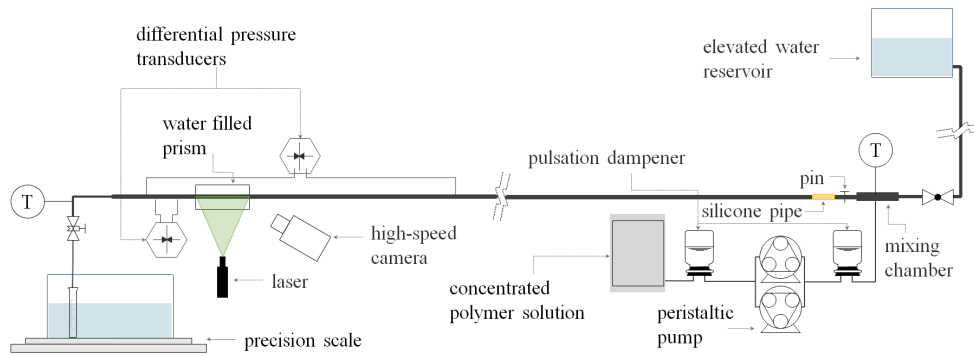


FIG. 6. Sketch of experimental setup; not to scale.

phase-offset peristaltic pumps through an air filled flow pulsation dampener. A second pulsation dampener and RTD probe were further added to the flexible piping between the pipe exit and the needle valve. A flexible silicone tube separating the mixing chamber from the glass pipe and a third pulsation dampener added to the inlet of the peristaltic pumps act in combination with the other dampeners to insure minimal vibrations and near zero flow pulsations as a result of polymer injection. The injected polymers are in the form of a 600ppm solution of polyacrylamide (PAM, molecular weight 5-6 million, Polysciences Europe GmbH, lot number: 685910) dissolved in water through a minimal shearing drum mixing process over several days and kept at 296K. Note that while the molecular weight is only slightly larger than that of polymers used by Samanta et al., the present batch was considerably more efficient at drag reduction. Partially this may be attributed to the changed mixing procedure, in contrast to Samanta et al. vigorous stirring was avoided in the present study in favor of the rotating drum technique which minimized degradation during the mixing phase. Premixed set concentrations of dilute polymer solutions were also tested in the same setup and these proved to be even more efficient than the injection method currently employed, however these results will not be discussed here apart from noting that overall the qualitative conclusions were consistent with what is presented here. In the current study, the concentration of polymers in

the pipe was adjusted by varying the injection rate of the concentrated polymer solution. The mixing chamber and the long development section of the pipe ensures homogeneous mixing of the concentrated polymer solution and the incoming water. The mixing efficiency of the polymers prior to the first pressure tap was tested by dyeing the concentrated solution and observing a homogeneous dye distribution far upstream of the tap. The measurement section begins at the first pressure tap and extends $132D$ in length ending at a second pressure tap for the differential pressure transducer dedicated to ascertaining the friction factor. A second differential pressure transducer was employed to measure pressure fluctuations along a $5D$ length of pipe. Laser Doppler velocimetry (LDV) and particle image velocimetry (PIV) measurements were performed through a water filled glass box around $87D$ from the first pressure tap using a section of pipe which had a refractive index similar to that of water. PIV measurements focused on the radial-axial cross section of the pipe. The PIV measurement window was $3D$ in length and images are mostly taken at a frequency of $\approx 70\text{Hz}$. The high time resolution allows us to reconstruct larger flow structures by stitching several images together while taking the structures convection speed into account (i.e. applying Taylors frozen turbulence hypothesis). Fluid exiting the pipe was collected and continuously weighed in order to assess the instantaneous mass flow rate, after which it was discarded.